PCCP

Accepted Manuscript

ROYAL SOCIETY OF CHEMISTRY

www.rsc.org/pccp

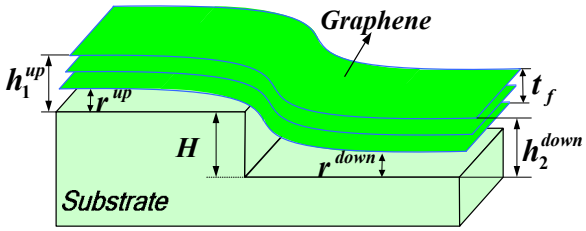

Thickness and substrate surface parameters dependence of interface adhesion properties of graphene membranes.

Effect of stepped substrates on the interfacial adhesion properties of graphene membranes

Yan He, Wangbing Yu and Gang Ouyang [a]

Key Laboratory of Low-Dimensional Quantum Structures and Quantum Control of the Ministry of Education, Department of Physics, Hunan Normal University, Changsha 410081, Hunan, China

Abstract

In order to gain a comprehensive understanding on interface adhesion properties involving in adhesion energy and local interface separation between graphene membranes and underlying stepped substrates, we develop an analytic model by considering the total free energy original from interfacial van der Waals interaction and elastic strain energy stored in the membranes based on atomic-bond-relaxation consideration. It is found that the interface adhesion energy decreases with increasing membrane thickness. Moreover, as compared to the case of flat substrate surface, the interface adhesion properties of graphene membranes on stepped surfaces have been strongly affected by the substrate surface parameters, including step height, vicinal angle, membrane thickness, terrace width and orientation, etc., implying that the topographic fluctuation of graphene is attributed to the various interface separation at different substrate sites. Our predictions agree reasonably well with the computer simulations and experimental observations, which suggest that the developed method can be regarded as an effective method to design the interface adhesion of graphene membranes in graphene-based functional device components.

[a] Corresponding author. E-mail address: gangouy@hunnu.edu.cn

Introduction

In recent years, graphene has become one of the focused problems in physics, chemistry and material science due to its charming properties and wide range of potential applications.[1,2] Conventionally, researchers prepared the high-quality graphene on various substrates such as metals and semiconductors in order to explore its exceptional performances.[3-5] Therefore, the interface properties between graphene and substrate contacts are very important and should be clarified in detail. So far, there are overwhelming investigations that have been made to pursue the interface properties including adhesion energy and interface separation from the aspects of experiment measurements and theoretical calculations.[3,6-9]

In general, the physical properties of graphene are strongly affected by the underlying substrate.[10-12] Recent work by Koenig *et al*.[3] experimentally measured that the interface adhesion energies between graphene and SiO_2 are 0.45±0.02 J/m^2 to 0.31±0.03 J/m^2 for the monolayer to multilayer with 2-5 layers. Yoon *et al*.[4] reported the adhesion energy between graphene and Cu is 0.72±0.07 J/m^2. Theoretically, Neel-Amal *et al*.[9] found the interface bond strength and the distribution of membrane strain are influenced by the morphologies of substrate surface (e.g., corrugated surface). Also, some other factors involved in substrate roughness, membrane thickness and surface forces have been taken into account on interface interaction of graphene and related systems. In particular, a kind of peculiar morphology such as sinusoid corrugation has also considered both experimentally and theoretically. For instance, Scharfenberg *et al*.[13-14] demonstrated the substrate morphology and membrane thickness have an effect on the interface adhesion energy in graphene systems. Gao *et al*.[15] predicted the interface adhesion energy can be related with the substrate roughness and amplitude. Moreover, they suggested that the van der Waals

interaction between graphene and substrate and the bending strain energy of graphene play the important roles for the adjustment of equilibrium graphene conformation. As a result, it is concluded that not only various types of substrates but also surface morphologies of substrates have significant effects on the interface adhesion properties.

However, the real morphology of substrate surface cannot usually be approached as an ideal flat surface and any other regulated period figures. For example, a real surface of substrates is rough and possesses many terraces and steps. A large number of un-flat or stepped substrate surfaces have been detected in experiment such as Cu,[16] Ir,[17] Ni,[18,19] SiC,[20,21] SiO_2[22,23] and so on. Subsequently, the stepped substrate will make the upper epitaxial layer has a big difference from that of the idea flat case.[24-26] Although many efforts have been employed to explore the interface and related properties in graphene membranes, there is still lacking a systematical study to illustrate the adhesion energy and interface separation for the graphene on stepped substrates from the atomistic origin. Furthermore, the influences of surface relaxation and interface mismatch on the interface interaction between graphene and underlying substrate are unclear so far.

In order to explore the relationship between the interface adhesion between graphene and the underlying substrate, in this work we present an analytic method to explore the issue by taking into account the free energies induced by membrane thickness and substrate surface parameters including terrace width and step height, etc., from the perspective of atomic-bond-relaxation mechanism. Interestingly, we find the anomalous interface adhesion energy and local interface separation are determined not only on the membrane thickness, but also on substrate surface parameters, which suggesting that the topographic fluctuation of graphene on stepped

substrates can be originally attributed to the unique interface adhesion behavior.

Principle

In order to address the influences of surface relaxation and interface mismatch effects as well as bending of membrane on the interfacial adhesion properties of graphene, we consider a multilayer graphene with volume V_0, area A_g, and thickness t_f on a stepped substrate surface, as depicted in Figure 1. In the figure 1(b) we show the geometric relationship regarding a bending graphene is placed at the step edge of substrate. Naturally, it can be divided into three regions (Figure 1(b)): I and III stand for the two terraces with different crystallographic orientation, while the region II denotes the bending deformation zone. Theoretically, the total free energy of the graphene membranes can be attributed to the contributions from the interfacial van der Waals interaction and the elastic strain energy stored in the membrane,

$$U_{total}^{(hkl)} = U_{vdw}^{(hkl)} + U_e \tag{1}$$

where $U_{vdw}^{(hkl)}$ is the interfacial potential energy between the graphene and the substrate in (hkl) crystallographic orientation. $U_e = U_e^{\phi}\left(\phi = \mathrm{I}, \mathrm{III}\right) + U_e^{\mathrm{II}}$ is the total elastic strain energy that includes the summation of deformation strain energy, U_e^{II}, (stored in II zone) and the strain energy, $U_e^{\phi}\left(\phi = \mathrm{I}, \mathrm{III}\right)$, (stored in I and III zones) due to interface and surface effects.

In our approach we only consider the interfacial van der Waals interaction energy is focused on the first layer and the substrate because almost 99% energy is concentrated in this area.[9] Thus, the interfacial potential energy can be written as, $W = \int_{A_g}\int_{V_s} W_{LJ}\rho_{s,(hkl)}\rho_g dV_s dA_g$, where $W_{LJ} = -C_1/r^6 + C_2/r^{12}$ is the van der Waals interaction between a carbon and a substrate atom, r is the distance between the two

atoms, C_1 and C_2 are the constants related to the material for the attractive and repulsive interactions, ρ_g and $\rho_{s,(hkl)}$ are the number of atoms per unit area of a monolayer graphene and the number of atoms per unit volume of the substrate in (hkl) orientation, V_s is the substrate volume. Consequently, the interfacial potential energy can be obtained,

$$U_{vdw}^{(hkl)} = -\Gamma_0^{(hkl)}\left[\frac{3}{2}\left(\frac{r_{0,(hkl)}}{r_{(hkl)}}\right)^3 - \frac{1}{2}\left(\frac{r_{0,(hkl)}}{r_{(hkl)}}\right)^9\right] \tag{2}$$

where $r_{0,(hkl)}$ is the interface separation under equilibrium, $\Gamma_0^{(hkl)} = \pi\rho_{s,(hkl)}\rho_g C_1 / 9r_{0,(hkl)}^3$ is the intrinsic adhesion energy per unit area in (hkl) of the bulk case.[27] In various crystallographic orientation the intrinsic adhesion energy can be calculated as following,

$$\frac{\Gamma_0^{(h_1k_1l_1)}}{\Gamma_0^{(h_2k_2l_2)}} = \frac{\rho_{s,(h_1k_1l_1)}}{\rho_{s,(h_2k_2l_2)}}\left(\frac{r_{0,(h_2k_2l_2)}}{r_{0,(h_1k_1l_1)}}\right)^3 \tag{3}$$

It is generally known that the performance of surface or edge atoms of nanosolids will dominate due to less coordination numbers (CNs) and stronger bonds with reduced size.[28,29] In particular, for the coherent bilayer systems consisting of graphene and rough substrate, the mismatch strain and associated with elastic energy will influence the stabilizing graphene and the critical graphene nucleus size.[30] Thus, the bilayer system will be in the self-equilibrium state due to surface and interface effects.[10,31,32] Commonly, the interface mismatch strain can be expressed as: $\varepsilon_{\text{int},(hkl)} = \left(a_{s,(hkl)} - a_f\right)/a_f$, where a_f and $a_{s,(hkl)}$ are the in-plane lattice constant of graphene and substrate in (hkl) orientation. In addition, the surface effect of epitaxial layers can be considered by atomic-bond-relaxation (ABR)

method.[29,33,34] Definitely, the key ideal ABR is that the bond less of an atom in the surface layer will result in the remaining bonds of the less-coordinated atom to shrink spontaneously. As a result, some relevant quantities such as densification of charge, mass, and bond energy will be different compared with those of the bulk counterparts and further impact the Hamiltonian and atomic cohesive energy, etc.

In combination with the surface and interface effects in graphene on substrate, the total strain in graphene membranes is

$$\varepsilon_f = \frac{\sum_{i<n} \varepsilon_i h_i + \varepsilon_{//,(hkl)} \ (t_f - \sum_{i<n} h_i)}{t_f} \tag{4}$$

where $\varepsilon_i = c_i - 1$ is the strain of the *i*th surface atomic layers, $\varepsilon_{//,(hkl)} = \varepsilon_{\text{int},(hkl)}(\varepsilon_{\text{int},(hkl)} + 1)h_0 / t_f$ is the strain in interface layers for (hkl) direction, h_i and h_0 represent the atomic bond length of the *i*th atomic layers and that of the bulk, *n* is the number of surface atomic layers, $c_i = 2/(1 + \exp((12 - z_i)/8z_i))$ denotes the CN-dependent bond contraction coefficient with z_i being the effective CNs in the *i*th atomic layer.[35,36] Noticeably, the thickness of multilayer graphene can be expressed as: $t_f = \sum_i c_i h_0$.

In our case we assume the substrate is rigid and the strain energy is primarily focused on the membranes. Therefore, in terms of continuum mechanics, the strain energy (per unit area) for the limiting case of interface confinement graphene is given by

$$U_e^{\phi}(\phi = \mathrm{I}, \mathrm{III}) = \frac{Y(t_f) t_f \varepsilon_f^2}{1 - \nu} \tag{5}$$

Here $Y(t_f)$ is the thickness-dependent Young's modulus of graphene membranes[34]

and $Y(t_f) = Y_B \left\{ \frac{z_b}{\langle z \rangle} \left[\sum_{i<n} \gamma_i \left(z_{ib} c_i^{-m} - 1 \right) + 1 \right] \left(1 + \varepsilon_f \right)^{-3} \right\}$. $z_{ib} = z_i / z_b$ and $\langle z \rangle = \gamma_i (z_i - z_b) + z_b$ are the CNs ratio between the *i*th atomic layer and that of the bulk, and the mean CNs, Y_B is the bulk Young's modulus, $m = 2.56$ is a index that characterizes the nature of carbon bonds, $\gamma_i = \sum_{i<n} c_i h_0 / t_f$ is the surface-to-volume ratio.

Additionally, we consider a multilayer graphene across the step edge is approximated by two identical arcs of cylinders with radius, R, and arc angle, θ_1, which a schematic illustration is depicted in Figure 1(b). Note that the curvature of bent graphene is not imposed but is the natural relaxation.[37] According to the theory of elasticity,[38] the moment *M* of membrane can be related to the Young's modulus and the curvature R, i.e., $M = Y(t_f) I / R$, where $I = L_x t_f^3 / 12$ is the moment of inertia with L_x being the length of terrace. Thus, the bending strain energy stored in the region II of graphene can be calculated

$$U_e^{\mathrm{II}} = 2 \int \frac{M^2 ds}{2YI} = \frac{Y(t_f) L_x t_f^2 \theta_1}{12} \ln \frac{R_0 + t_f}{R_0} \tag{6}$$

where R_0 and s are the radius of the innermost layer of graphene and the arc length of region II depicted in the Figure 1(b).

Consider the lattice strain induced by surface relaxation and interface misfit, as well as the van der Waals interaction between graphene and a substrate, the relationship between the critical interface separation $r^*_{(hkl)}$ in (hkl) direction and the membrane thickness t_f should be obtained by setting $\partial U_{total}^{(hkl)} / \partial h_{(hkl)} = \partial U_{vdw}^{(hkl)} / \partial r_{(hkl)} + \partial U_e / \partial t_f$. Thus, we have

$$\left(\frac{r_{0,\ (hkl)}}{r^*_{(hkl)}}\right)^{10}-\left(\frac{r_{0,\ (hkl)}}{r^*_{(hkl)}}\right)^{4}=\frac{2r_{0,\ (hkl)}}{9\Gamma_0^{(hkl)}}\frac{\partial U_e}{\partial t_f} \tag{7}$$

with

$$\frac{\partial U_e}{\partial t_f}=\frac{\sum S_\varphi \partial U_e^\phi/\partial t_f+S_{\rm II}U_e^\phi/R-\partial U_e^{\rm II}/\partial t_f}{\sum S_\varphi}-\frac{\left(\sum S_\varphi U_e^\phi-U_e^{\rm II}\right)S_{\rm II}/R}{\left(\sum S_\varphi\right)^2},$$

$$\frac{\partial U_e^\phi}{\partial t_f}=\frac{t_f\varepsilon_f^2}{1-\nu}\frac{\partial Y\left(t_f\right)}{\partial t_f}+\frac{\varepsilon_f^2}{1-\nu}Y(t_f)+\frac{2Y(t_f)(\varepsilon_{//}-\varepsilon_f)\varepsilon_f}{1-\nu},$$

$$\frac{\partial U_e^{\rm II}}{\partial t_f}=\frac{L_x t_f^2\theta_1}{12}\ln\frac{R_0+t_f}{R_0}\frac{\partial Y\left(t_f\right)}{\partial t_f}+\frac{Y\left(t_f\right)L_x t_f\theta_1}{6}\ln\frac{R_0+t_f}{R_0}+\frac{Y\left(t_f\right)L_x t_f^2\theta_1}{12\left(R_0+t_f\right)},$$

and

$$\frac{\partial Y(t_f)}{\partial t_f}=\frac{Y\left(t_f\right)}{t_f}\left\{\sum_{i<n}\frac{\gamma_i(z_i-z_b)}{\left\langle z\right\rangle}-\frac{1}{1+\left[\sum_{i<n}\gamma_i\left(z_{ib}c_i^{-m}-1\right)\right]^{-1}}-\frac{3(\varepsilon_{//}-\varepsilon_f)}{(1+\varepsilon_f)}\right\}$$

where $S_\varphi(\varphi=\mathrm{I},\mathrm{II},\mathrm{III})$ represent the I, II and III regions. It should be indicated that the $S_{\rm II}=2R\theta_1L_x$, where $R=R_0+t_f/2$ is the radius of middle layer of membrane shown in Figure 1(c).

As a result, by considering the total strain from the surface and interface effects as well as the deformation and the van der Waals interactions, the total free energy for graphene on stepped substrate surfaces in self-equilibrium state can be obtained:

$$\tilde{U}=-\sum\Gamma_0^{(hkl)}\left[\frac{3}{2}\left(\frac{r_{0,\ (hkl)}}{r^*_{(hkl)}}\right)^3-\frac{1}{2}\left(\frac{r_{0,\ (hkl)}}{r^*_{(hkl)}}\right)^9\right]-\frac{\frac{Y(t_f)t_f\varepsilon_f^2}{1-\nu}\sum S_\varphi-U_e^{\rm II}}{\sum S_\varphi} \tag{8}$$

Results and discussion

Hemandez *et al.*[39] pointed out that the well-defined parameterization of bulk

graphite (e.g., a Young's modulus of 1.02 TPa) cannot be suitable for the case of graphene. In fact, the thickness dependence of Young's moduli of graphene membranes have been achieved from both experimentally and theoretically.[40,41] Apparently, the Young's modulus of grahpene is an important parameter that determines the interface adhesion properties. Therefore, in our case we first calculate the Young's modulus of graphene membranes and the results are shown in Figure 2. Note that the related parameters used in calculations are given in Table 1. Clearly, the Young's moduli of graphene membranes from 1-5 layers, respectively, are 3.14, 1.71, 1.41, 1.29 and 1.23 TPa, which increase dramatically with decreasing membrane thickness. The symbols shown in Figure 2 mean the relevant experimental and theoretical results[40,41] that are well agreement with our predictions.

In nature, the underlying substrate surface parameters, including terrace width and step height, will affect the interfacial adhesion properties of the upper epitaxial layer. In terms of the geometric relationship depicted in Figure 1(c), the bending of graphene at the step edge necessarily induces a Δ_C shift in the graphene structure perpendicular to the step edges. There exists a geometric relationship:[17] $H/2 = R(1-\cos\theta_1)$ and $\Delta_C = 2R\sin\theta_1 - 2R\theta_1 + kd_{CC}$, where H and $d_{CC}(=\sqrt{3}a_f)$ are the step height and the carbon period along the bending direction, k is the integer number of carbon rings that takes the integer part of H/d_{CC}, and $k=0$ if $H \le d_{CC}$. Therefore, we obtain the relation as $\sqrt{(k+1)^2 d_{CC}^2 - H^2} - d_{CC} \le \Delta_C \le 0$ and further get the average values of R and θ_1. In our calculation we get the values of R are 23.3, 35.3, and 72.9 nm when $H = 0.5$, 0.349 and 0.174 nm, respectively.

Based on Eq.(8), the total free energy of graphene placed on SiO_2(001) at fixed

terrace width 300 nm and step height 0.5 nm under different vicinal angles θ_2 is calculated and the results are shown in Figure 3. Strikingly, we find that the minima of total free energies have obvious shift with number of layers and is a function of substrate surface parameters. Physically, this is attributed to the graphene membrane thickness-dependent Young's modulus that can be modulated by elastic strain energies stored in membrane.[42]

Aim at gaining a better understanding of the interface separation in graphene/SiO_2(001), we extract the critical values from Figure 3 and re-describe the variant trend as shown in Figure 4(a). It is clear to show that the interface separation becomes larger with increasing number of layers and vicinal angles. Interestingly, the interface separation is larger than the intrinsic equilibrium distance as the membrane thickness increased. In fact, these results can be attributed to the changes of geometrical parameters of substrate surface. When the vicinal angle becomes larger, the step height will be higher at fixed terrace width, whereas the terrace width becomes smaller at fixed step height. Both of these two cases lead to the enhancement of bending elastic energy stored in membranes and result in the variation of interface separation. Notably, the interaction between graphene and edge step (vertical to the terrace surface) in II zone can be generally ignored. It is concluded that the contribution of bending strain energy to the total free energy is pronounced than that of energy induced by the surface relaxation and interface mismatch when both terrace width and step height increase at fixed vicinal angle. Aitken *et al*.[27] reported that the bending strain energy of graphene has an ineffaceable contribution to the interface separation, and they found the interface separation changes with variation of elastic strain energy, which is consistent with our calculations.

Theoretically, the interface adhesion energy is related to the total free energy at

the equilibrium state, i.e., $\Gamma = -\tilde{U}$. As illustrated in Figure 4(b), the interface adhesion energy is shown as a function of number of layers, terrace width, edge height and vicinal angles. Apparently, the interface adhesion energy increases with a reduction in membrane thickness, which is in accord with the experimental observations.[3] Also, the adhesion energy has a slight change with different vicinal angles from monolayer to trilayer of graphene unless the number of layers reach or more than fourth. It is mainly due to the bending strain energy is much smaller than the surface and interface strain energies stored in monolayer to trilayer graphene. When the graphene layers increase, the bending strain energy becomes larger and the surface and interface strain energies will be diminishing, thus leads the adhesion energy will be different with varying vicinal angles. On the other hand, we find the interface adhesion energy decreases with increasing vicinal angles at fixed terrace width and step height. For example, in the case of bilayer graphene the adhesion energies are, respectively, 0.355, 0.352, 0.349, 0.345 J/m^2 at fixed terrace width 300 nm, and 0.355, 0.354, 0.351, 0.345 J/m^2 at fixed step height 0.5 nm under the condition of vicinal angles range from 0° to 0.1°. Gao *et al.*[15] reported that the interface adhesion energy would be diminishing with enhancement the roughness of substrate (e.g., sinusoidal surface with surface amplitude δ_s). Noticeably, the symbols shown in Figure 4(b) mean the cases from both planar[3] and sinusoidal substrate surfaces.[15] Evidently, the general trends of our predictions agree well with Gao and co-workers' results.[15] Moreover, in our approach we further consider the surface relaxation and interface mismatch effects and find the interface adhesion energy can be tuned by the underlying substrate surface parameters.

In order to further demonstrate the consistency of our analysis, we consider a multilayer graphene placed on Cu (111) with two different stacking modes in up- and

down-terrace, as shown in Figure 5(a). Using Eq.(3) and through setting $\Gamma_0^{up} = 13.19$ meV/Å^2, $r_0^{up} = 0.326$ nm,[43] and a fixed interface separation of the down-terrace, $r_0^{down} = 0.224$ nm, we obtain $\Gamma_0^{down} = 18.88$ meV/Å^2, which is very close to the top-hcp structure, 20.2 meV/Å^2 reported by Xu and Buehler's calculations.[43] Under these circumstances, the critical interface separation and the interface adhesion energy can be calculated by Eqs.(7) and (8).

Figure 5(a) also shows the relationship among critical interface separation, number of graphene layers, different stacking modes in up- and down-terrace and step heights. Clearly, the critical interface separations in both of two cases increase with rising number of graphene layers, and even beyond the intrinsic interface separation under the flat surface if the underlying substrate surface exists steps. By contrast, the interface separation in up-terrace is larger than that of down-terrace, which is due to various interface binding energy and associated with the existing of elastic strain energies in two different stacking modes. In addition, from the comparison of interface separation in graphene/Cu and graphene/SiO_2, we find the main difference of two cases: (i) the shift of interface separation in graphene/Cu will take place when the membrane thicknesses beyond 4 layers, while that in graphene/SiO_2 is 3 layers, and (ii) the interface separation in graphene/Cu is less than that in graphene/SiO_2. This is due to the different mismatch strain energy, interfaces bonding energy and intrinsic interface separation of the two systems.[44] Moreover, as plotted on Figure 5(a), when the step height becomes zero, i.e. $H = 0$ nm, the results are consistent with the case of flat substrate surface.[11]

The corresponding interface adhesion energy in graphene/Cu is shown in Figure 5(b). Similarly, it shows an evident thickness effect and can be determined by the substrate surface parameters such as terrace width and step height. For instance, the

adhesion energy increases with diminishing terrace width. Also, the adhesion energy increases with the step height, which is similar to Figure 4(b). It should be noted that the case is the same as the flat surface when we fixed $H = 0$ nm, $L_{terrace}^{up} = 300$ nm, and $L_{terrace}^{down} = 0$ nm, which agree with the experimental measurements reported by Yoon *et al*.[4] Note that the star symbol shown in Figure 5(b) means the measurable value from Yoon *et al.*[4]

Remarkably, we find that the interface adhesion energy is approximately equal to zero when the thickness reach to 10 layers as plotted in Figure 5(b), indicating that the graphene will detach from the substrate with an increase of membrane thickness. Thus, the detachment of graphene on a stepped substrate is determined on the underlying substrate surface parameters, including terrace orientation, terrace width and height, etc. Scharfenberg *et al*.[14] observed that the graphene undergoes a sharp snap-through transition between conforming to the substrate and lying on top of the substrate with sinusoidal surface at a critical layers, which implies that the adhesion energy becomes weaker and the graphene can be extracted easily. Besides, Li and co-workers[45-48] found that the detachment of graphene on Si nanosolids (e.g., nanowire and nanoparticle) is determined on interface bonding energy, diameter and interspacing between two nanosolids. Therefore, our predictions are in accordance with these evidences, suggesting that the developed method can be as an effective tool for tailoring the related mechanical properties of graphene to the desired applications.

Conclusions and outlook

We establish an analytic method to explore the interface adhesion properties in graphene membranes from the perspective of atomistic origin. As examples we analyzed two types of systems, i.e., graphene/SiO_2 and graphene/Cu and found that

the effects of the adhesion energy and local interface separation at self-equilibrium state on the underlying substrate parameters, including steps height, vicinal angle, terrace width, and membrane thickness, etc. It is demonstrated that the surface relaxation and interface mismatch and associated with elastic strain energy stored in the graphene membranes affect the physical properties such as the Young's modulus and the local interface separation. In addition, we predict an effective way to extract graphene from the underlying substrate through modifying the substrate surface parameters (e.g., steps height, terrace width, and the substrate surface orientation.). Our results agree reasonably well with the theoretical calculations and the experimental measurements. Therefore, we expect that the developed method could be regarded as a theoretical tool to design the interface adhesion of graphene membranes in graphene-based nanomechanical and nanoelectronic devices.

Acknowledgements

This work was supported by the National Natural Science Foundation of China (Grant Nos. 11174076 and 91233203), the Hunan Provincial Natural Science Foundation of China (Nos. 12JJ1009 and 11JJ7001)) and Scientific Research Fund of Hunan Provincial Education Department (No. 12A082).

References

1 A. K. Geim, *Science*, 2009, **324**, 1530.

2 N. A. H. Castno, F. Guinea, N. M. R. Penes, K. S. Novoselov and A. K. Geim, *Rev. Mod. Phys.*, 2009, **81**, 109.

3 S. P. Koenig, N. G. Boddeti, M. L. Dunn and J. S. Bunch, *Nat. Nanotech.*, 2011, **6**, 543.

4 T. Yoon, W. C. Shin, T. Y. Kim, J. H. Mun, T. Kim and B. J. Cho, *Nano Lett.*, 2012, **12**, 1448.

5 Y. Ogawa, B. Hu, C. M. Orofeo, M. Tsuji, K. Ikeda, S. Mizuno, H. Hibino and H. Ago, *J. Phys. Chem. Lett.*, 2012, **3**, 219.

6 S. Xia and L. Ponson, *Phys. Rev. Lett.*, 2012, **108**, 196101.

7 S. Das, D. Lahiri, D. Y. Lee, A. Agarwal and W. Choi, *Carbon*, 2013, **59**, 121.

8 T. S. Chow, *Phys. Rev. Lett.*, 2011, **86**, 4592.

9 M. Neek-Amal and F. M. Peeters, *Phys. Rev. B*, 2012, **85**, 195445.

10 J. Zheng, Y. Wang, L. Wang, R. Quhe, Z. Ni, W. N. Mei, Z. Gao, D. Yu, J. Shi and J. Lu, *Sci. Rep.*, 2013, **3**, 2081.

11 Y. He, W. F. Chen, W. B. Yu, G. Ouyang and G. W. Yang, *Sci. Rep.*, 2013, **3**, 2660.

12 Y. Kim, J. Lee, M. S. Yeom, J. W. Shin, H. Kim, Y. Cui, J. W. Kysar, J. Hone, Y. Jung, S. Jeon and S. M. Han, *Nat. Commun.*, 2013, **4**, 2114.

13 S. Scharfenberg, D. Z. Rocklin, C. Chialvo, R. L. Weaver, P. M. Goldbart and N. Mason, *Appl. Phys. Lett.*, 2011, **98**, 091908.

14 S. Scharfenberg, N. Mansukhani, C. Cesar, R. Weaver and N. Mason, *Appl. Phys. Lett.*, 2012, **100**, 021910.

15 W. Gao and R. Huang, *J. Phys. D: Appl. Phys.*, 2011, **44**, 452001.

16 H. I. Rasool, E. B. Song, M. J. Allen, J. K. Wassei, R. B. Kaner, K. L. Wang, B. H.

Weiller and J. K. Gimaewski, *Nano Lett.*, 2011, **11**, 251.

17 J. Coraux, A. T. N'Diaye, C. Busse and T. Michely, *Nano Lett.*, 2008, **8**, 565.

18 Y. F. Zhang, T. Gao, S. B. Xie, B. Y. Dai, L. Fu, Y. B. Gao, Y. B. Chen, M. X. Liu and Z. F. Liu, *Nano Res.*, 2012, **5**, 402.

19 J. F. Gao, J. Yip, J. J. Zhao, B. I. Yakobson and F. Ding, *J. Am. Chem. Soc.*, 2011, **133**, 5009.

20 P. Lauffer, K. V. Emtsev, R. Graupner, Th Seyller and L. Ley, *Phys. Rev. B*, 2008, **77**, 155426.

21 M. L. Bolen, S. E. Harrison, L. B. Biedermann and M. Capano, *Phys. Rev. B*, 2009, **80**, 115433.

22 N. Tokuda, M. Murata, D. Hojo and K. Yamabe, *Jpn. J. Appl. Phys.*, 2001, **40**, 4763.

23 D. J. Bottomley, H. Omi, Y. Kobayashi, M. Uemastsu, H. Kageshima and T. Ogino, *Phys. Rev. B*, 2002, **66**, 035301.

24 V. M. Pereira and N. A. H. Castro, *Phys. Rev. Lett.*, 2009, **103**, 046801.

25 W. G. Cullen, M. Yamamoto, K. M. Burson, J. H. Chen, C. Jang, L. Li, M. S. Fuhrer and E. D. Williams, *Phys. Rev. Lett.*, 2010, **105**, 215504.

26 Q. H. Wang, Z. Jin, K. K. Kim, A. J. Hilmer, G. L. C. Paulus, C. J. Shih, M. H. Ham, J. D. Sanchez-Yamagishi, K. Watanabe, T. Taniguchi, J. Kong, P. J. Jarillo-Herrero and M. S. Strano, *Nat. Chem.*, 2012, **4**, 724.

27 Z. H. Aitken and R. Huang, *J. Appl. Phys.*, 2010, **107**, 123531.

28 G. Ouyang, G. W. Yang and G. H. Zhou, *Nanoscale*, 2012, **4**, 2748.

29 C. Q. Sun, *Prog. Mater. Sci.*, 2007, **35**, 1.

30 S. Saadi, F. Abild-Pedersen, S. Helveg, J. Sehested, B. Hinnemann, C. C. Appel and J. K. Nørskov, *J. Phys. Chem. C*, 2010, **114**, 11221.

31 Z. M. Zhu, A. Zhang, Y. He, G. Ouyang and G. W. Yang, *AIP Advances*, 2012, **2**, 042185.

32 G. Ouyang, C. X. Wang and G. W. Yang, *Chem. Rev.*, 2009, **109**, 4221.

33 A. Zhang, Z. M. Zhu, Y. He and G. Ouyang, *Appl. Phys. Lett.*, 2012, **100**, 171912.

34 G. Ouyang, W. G. Zhu, C. Q. Sun, Z. M. Zhu and S. Z. Liao, *Phys. Chem. Chem. Phys.*, 2010, **12**, 1543.

35 Z. M. Zhu, A. Zhang, G. Ouyang and G. W. Yang, *J. Phys. Chem. C,* 2011, **115**, 6462.

36 X. X. Yang, J. W. Li, Z. F. Zhou, Y. Wang, L. W. Yang and W. T. Zheng and C. Q. Sun, *Nanoscale*, 2012, **4**, 502.

37 I. Nikiforov, D. B. Zhang, R. D. James and T. Dumitrică, *Appl. Phys. Lett.*, 2010, **96**, 123107.

38 G. G. Tibbetts, *J. Cryst. Growth*, 1984, **66**, 632.

39 E. Hernández, C. Goze, P. Bernier and A. Rubio, *Phys. Rev. Lett.*, 1998, **80**, 4502.

40 D. B. Zhang, E. Akatyeva and T. Dumitrică, *Phys. Rev. Lett.*, 2011, **106**, 255503.

41 J. U. Lee, D. Yoon and H. Cheong, *Nano Lett.* 2012, **12**, 4444.

42 M. Poot and H. S. J. van der Zant, *Appl. Phys. Lett.* 2008, **92**, 063111.

43 Z. Xu and M. J. Buehler, *J. Phys. Condense Matter* 2010, **22**, 485301.

44 L. Y. Jiang, Y. Huang, H. Jiang, G. Ravichandran, H. Gao, K. C. Hwang, B. Liu, *J. Mech. Phys. Solids*, 2006, **54**, 2436.

45 T. Li and Z. Zhang, *Nanoscale Res. Lett.*, 2010, **5**, 169.

46 Z. Zhang and T. Li, *J. Appl. Phys.*, 2010, **107**, 103519.

47 T. Li, *Modelling Simul. Mater. Sci. Eng.*, 2011, **19**, 054005.

48 S. Z. Zhu and T. Li, *J. Appl. Mech.*, 2014, **81**, 061008.

49 C. Lee, X. Wei, J. W. Kysar and J. Hone, *Science*, 2008, **321**, 385.

50 M. Z. Hossain, *Appl. Phys. Lett.*, 2009, **95**, 143125.

51 G. Giovannetti, P. A. Khomyakov, G. Brocks, V. M. Karpan, J. van den Brink and P. J. Kelly, *Phys. Rev. Lett.*, 2008, **101**, 026803.

52 V. Dmitriev, V. Torgashev, P. Toledano and E. K. H. Salje, *Europhys. Lett.*, 1997, **37**, 553.

Table 1. Input parameters for calculations. r_0, a, h_0, E, ν and Y_B are the interface equilibrium distance, in-plane lattice constant, bond length, binding energy per unit area, Poisson's ratio and Young's modulus, respectively.

	r_0 [nm]	a [nm]	h_0 [nm]	E [meV/Å^2]	ν	Y_B [TPa]
Graphene	0.34[49]	0.2445[51]	0.142[4]		0.16[3]	1.02[49]
Cu		0.361[43]				
SiO_2		0.499[52]				
Graphene/SiO_2	0.3[50]			17.01[50]		

Figure Captions

Figure 1. (a) Schematic illustration showing a multilayer graphene on a stepped substrate surface. t_f is the thickness of graphene membrane, r^{up} and r^{down} are the interface separations between graphene and substrate in up- and down-terrace surface, $h_1^{up} = r^{up} + t_f$ and $h_2^{down} = r^{down} + t_f$ represent the heights between the top layer of graphene and the substrate in two different terrace surface. (b) Geometric relationship about the multilayer graphene on the stepped surface. θ_1 and θ_2 , respectively, are the central angle due to the bending of graphene and the vicinal angle. The regions I, II and III correspond to the flat and step areas of the substrate. (c) Schematic illustration of a change in position of carbon atoms located at the edge of step.

Figure 2. The solid line denotes our predictions, while the symbols mean the available evidences.

Figure 3. The relationship among total free energy, number of layers and interface separation of graphene/SiO_2 under (a) $L(001) = 300\ nm$ and (b) $H = 0.5\ nm$ at fixed vicinal angles, $\theta_2 = 0^\circ, 0.033^0, 0.067^0$ and 0.1^0.

Figure 4. Dependence of critical interface separation (a) and interface adhesion energy (b) on the membrane thickness, vicinal angle and terrace width for graphene/SiO_2.

Figure 5. Dependence of critical interface separation (a) and interface adhesion energy (b) on the membrane thickness, vicinal angle, step height, terrace width and crystalline orientation for graphene/Cu. Note that the structures considered for

graphene/Cu surface seen from the left side of (a) and the color codes for carbon and copper atoms are black and brown, respectively.

Figure 1

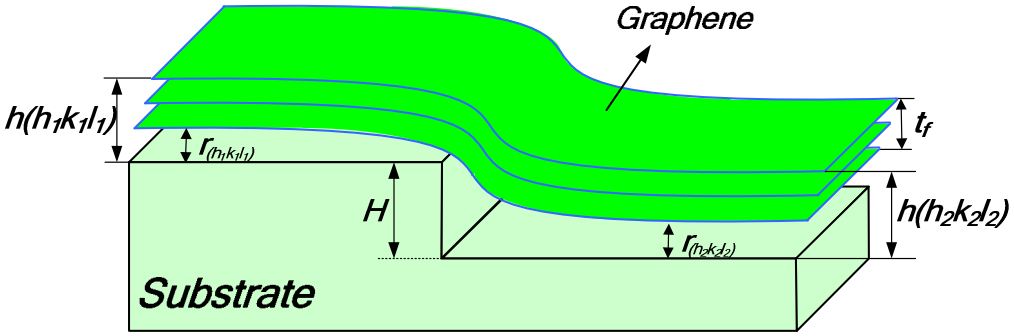

(a)

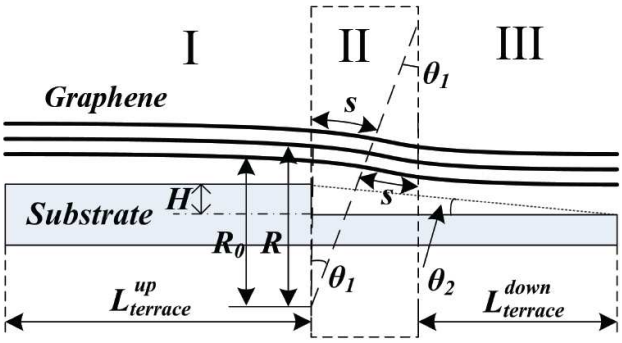

(b)

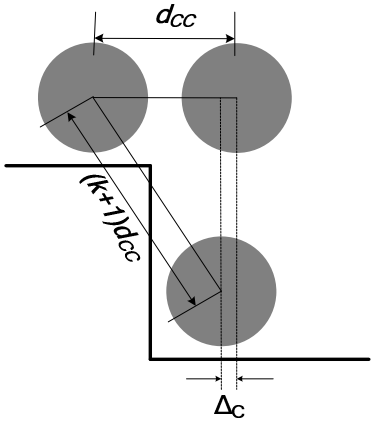

(c)

Figure 2

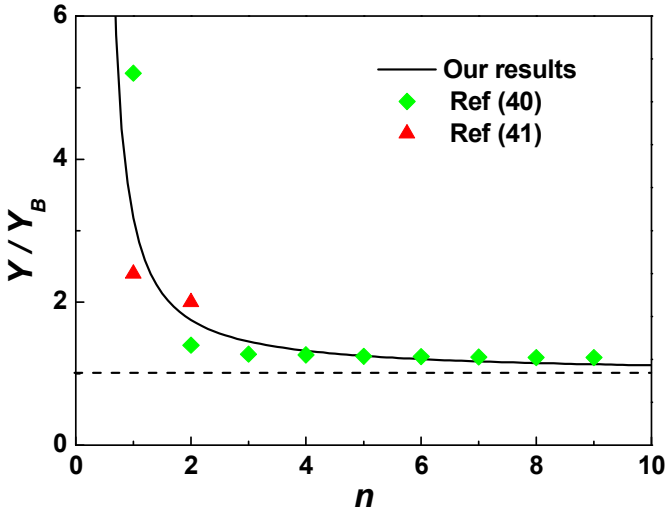

Figure 3

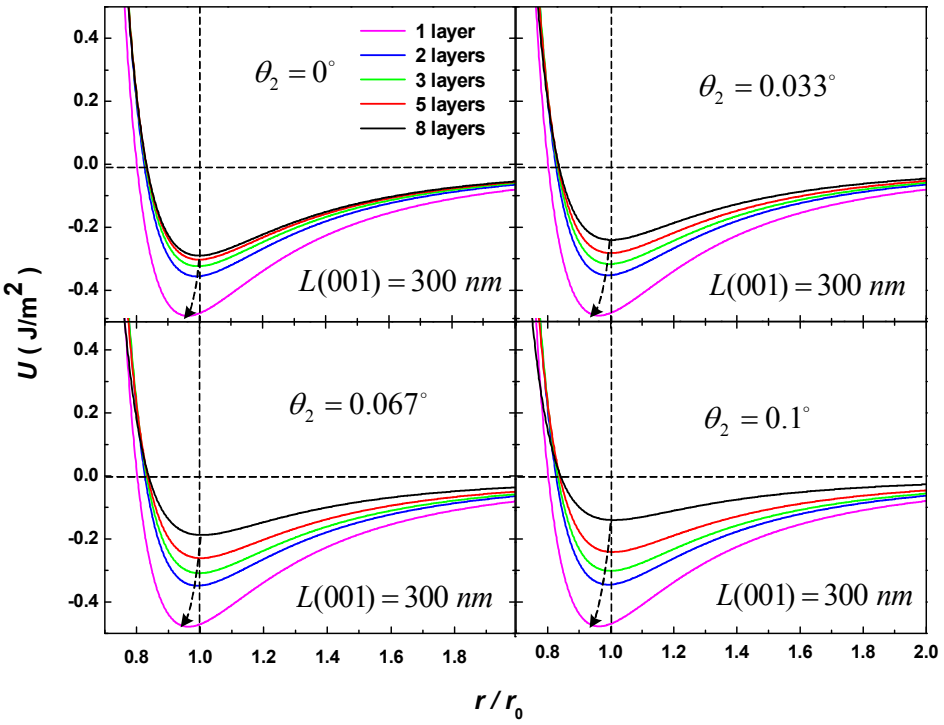

(a)

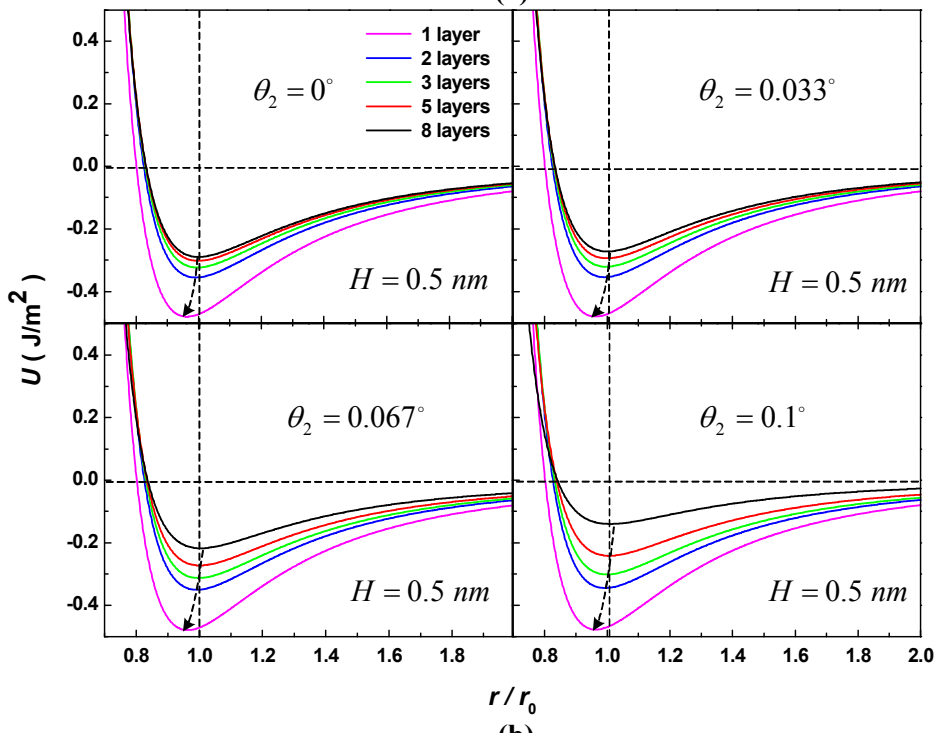

(b)

Figure 4

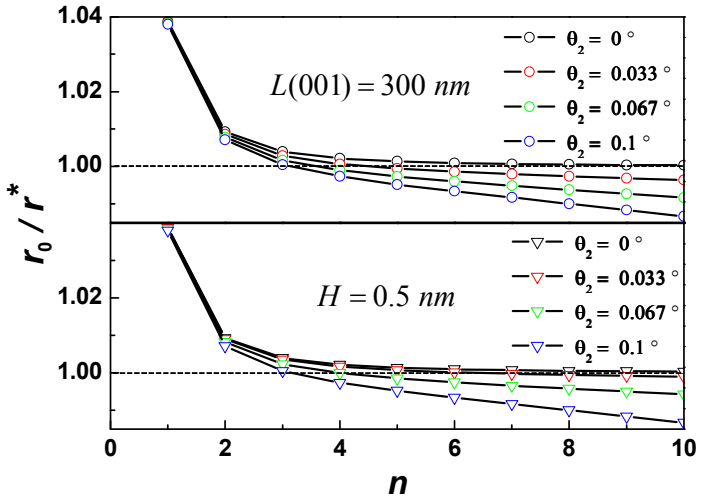

(a)

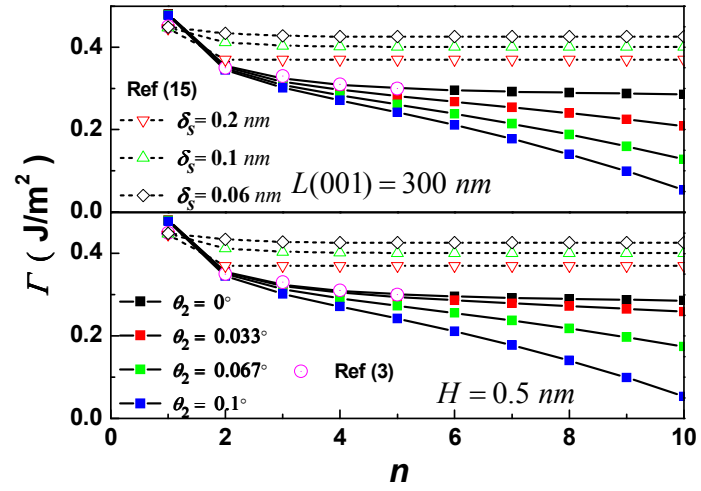

(b)

Figure 5

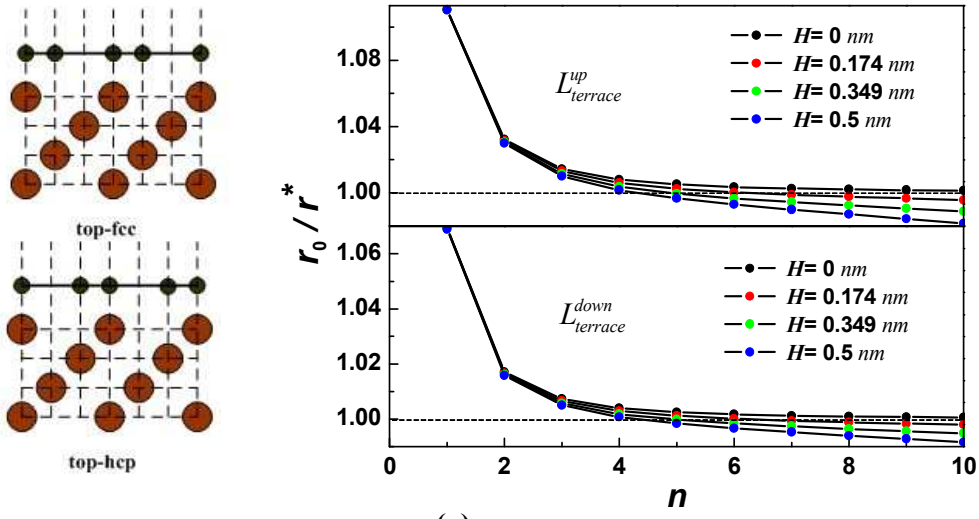

(a)

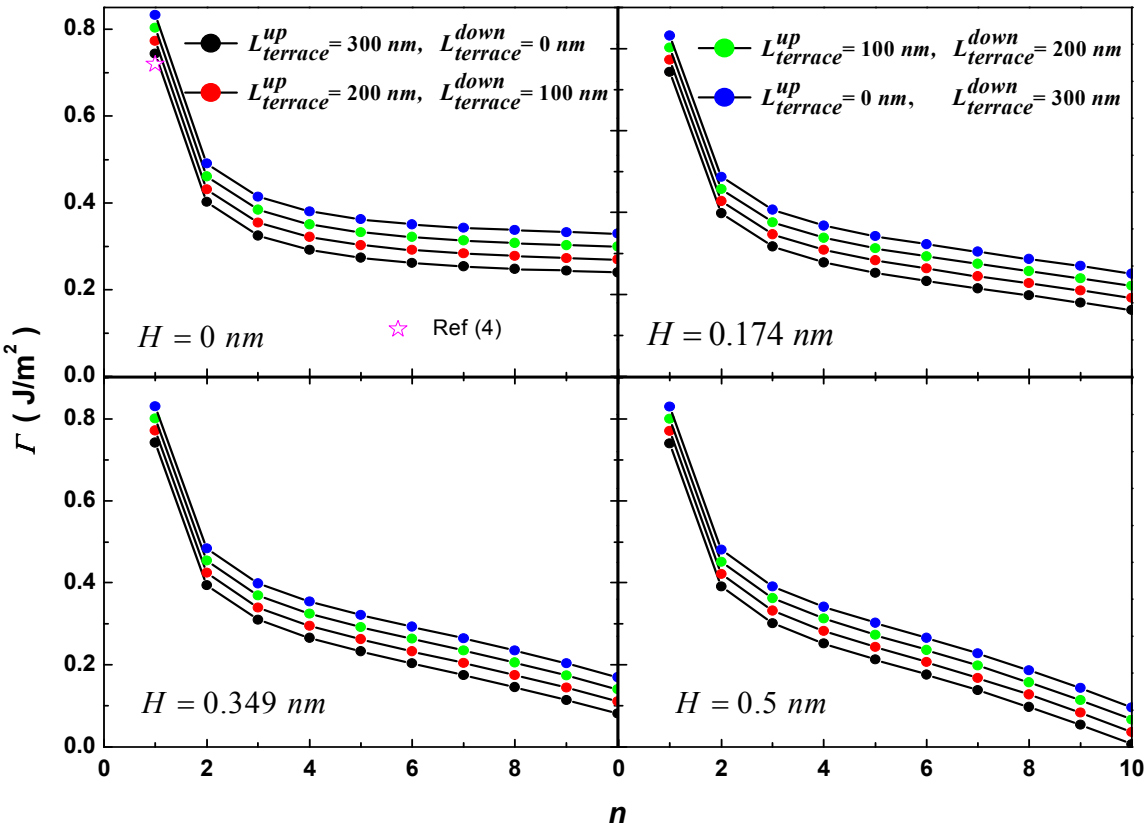

(b)